

Multi-Exit Semantic Segmentation Networks

Alexandros Kouris¹, Stylianos I. Venieris¹, Stefanos Laskaridis¹, Nicholas D. Lane^{1,2}
¹Samsung AI Center, Cambridge ²University of Cambridge

{a.kouris,s.venieris,stefanos.l,nic.lane}@samsung.com

Abstract

Semantic segmentation arises as the backbone of many vision systems, spanning from self-driving cars and robot navigation to augmented reality and teleconferencing. Frequently operating under stringent latency constraints within a limited resource envelope, optimising for efficient execution becomes important. To this end, we propose a framework for converting state-of-the-art segmentation models to MESS networks; specially trained CNNs that employ parametrised early exits along their depth to save computation during inference on easier samples. Designing and training such networks naively can hurt performance. Thus, we propose a two-staged training process that pushes semantically important features early in the network. We co-optimize the number, placement and architecture of the attached segmentation heads, along with the exit policy, to adapt to the device capabilities and application-specific requirements. Optimising for speed, MESS networks can achieve latency gains of up to $2.83\times$ over state-of-the-art methods with no accuracy degradation. Accordingly, optimising for accuracy, we achieve an improvement of up to 5.33 pp, under the same computational budget.

1. Introduction

Semantic segmentation constitutes a core machine vision task that has demonstrated tremendous advancement due to the emergence of deep learning [15]. By predicting dense (every-pixel) semantic labels for an image of arbitrary resolution, semantic segmentation forms one of the finest-grained visual scene understanding tasks, materialised as an enabling technology for myriad applications, including augmented reality [35, 64], video conferencing [69, 45], navigation [50, 62], and semantic mapping [40]. Quality-of-service and safety are of utmost importance when deploying such real-time systems, typically running on resource-constrained platforms [22, 64], spanning smartphones, consumer robots and self-driving cars. Thus, efficient and accurate segmentation becomes a core problem to solve.

State-of-the-art semantic segmentation models, however, pose their own challenges, as their impressive accuracy comes at the cost of excessive computational and memory demands. Particularly, the every-pixel nature of the seg-

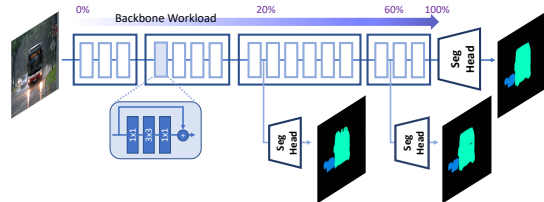


Figure 1: Multi-exit semantic segmentation network instance.

mentation output calls for high-resolution feature maps to be preserved throughout the network (to avoid the eradication of spatial information), while also maintaining a large receptive field on the output (to incorporate context and achieve robust semantic predictions) [46]. Thus, the resulting network architectures typically consist of numerous layers and frequently replace feature-volume downsampling with dilated convolutions of increasing rate [67], leading to significant workload concentration deeper in the network, which, in turn, results in latency-intensive inference.

Alleviating this latency burden is important, especially for edge deployment on resource-constrained platforms [1]. To this direction, recent work has focused on the design of lightweight segmentation models either manually [41, 73] or through Neural Architecture Search [34]. Simultaneously, advances in adaptive DNN inference, offering complementary gains by dynamically adjusting the computation path in an input-dependent manner, have been aimed at image classification [20, 24, 75], leaving challenges in segmentation largely unaddressed. In fact, naively applying early exiting on segmentation CNNs can lead to degraded accuracy due to early-exit “cross-talk” during training, and potential zero latency gains due to the inherently heavyweight architecture of segmentation heads. For example, naively adding a single segmentation head on DeepLabV3 [6] can lead to an overhead of up to 40% of the original model’s workload. Equally important, the dense output of segmentation models further complicates the exit-policy.

In this work, we introduce the MESS framework, a novel methodology for deriving and training Multi-Exit Semantic Segmentation (MESS) networks from a user-defined architecture for efficient segmentation, tailored to the device and task at hand. Given a CNN, MESS treats it as a backbone architecture and attaches numerous “early exits”

(i.e. segmentation heads) at different depths (Fig. 1), offering predictions with varying workload-accuracy characteristics. Importantly, the architecture, number and placement of early exits remain configurable and can be co-optimised via search upon deployment to target devices of different capabilities and application requirements, without the need to retrain, leading to a train-once, deploy-everywhere paradigm. This way, MESS can support various inference pipelines, ranging from sub-network extraction to progressive refinement of predictions and confidence-based exiting. The main contributions of this work are the following:

- The design of MESS networks, combining adaptive inference through early exits with architecture customisation, to provide a fine granularity speed-accuracy trade-off, tailor-made for semantic segmentation tasks. This allows for efficient inference based on the input’s difficulty and the target device’s capabilities.
- A two-stage scheme for training MESS networks, starting with an exit-aware end-to-end training of an overprovisioned network, followed by a frozen-backbone distillation-based refinement for training all candidate early exit architectures. This mechanism boosts the accuracy of MESS networks and disentangles the training from the deployment configuration.
- An input-dependent inference pipeline for MESS networks, employing a novel method for estimating the prediction confidence at each exit, tailored for every-pixel outputs. This mechanism enables difficulty-based allocation of resources, by early-stopping for “easy” inputs with corresponding performance gains.

2. Related Work

Efficient Segmentation. Semantic segmentation is rapidly evolving, since the emergence of the first CNN-based approaches [37, 2, 43, 48]. Recent advances have focused on optimising accuracy through stronger backbone CNNs [17, 21], dilated convolutions [67, 5], multi-scale processing [66, 74] and multi-path refinement [31, 14]. To reduce the computational cost, the design of lightweight hand-crafted [41, 57, 73, 65] and more recently via NAS-crafted [42, 34, 70] architectures has been explored, with further efforts to compensate for the lost accuracy through knowledge distillation [36] or adversarial training [39]. Our framework is model-agnostic and can be applied on top of existent CNN backbones – lightweight or not – achieving significant complementary gains through the orthogonal dimension of input-dependent (dynamic) path selection.

Adaptive Inference. The key paradigm behind adaptive inference is to save computation on “easy” samples, thus reducing the overall computation time with minimal impact on accuracy [3, 12]. Existing methods in this direction can be taxonomised into: 1) Dynamic routing networks selecting a different sequence of operations to run in an input-

dependent way, by skipping either layers [53, 55, 59] or channels [32, 19, 11, 13, 56] and 2) Multi-exit networks [52, 20, 26, 60, 61, 68] forming a class of architectures with intermediate classifiers along their depths. With earlier exits running faster and deeper ones being more accurate, such networks provide varying accuracy-cost trade-offs. Existing work has mainly focused on image classification, proposing hand-crafted [20, 72], model-agnostic [52, 24] and deployment-aware architectures [25, 26]. However, the adoption of these techniques in segmentation models poses additional, yet unexplored, challenges.

Adaptive Segmentation Networks. Recently, initial efforts on adaptive segmentation have been presented. Li et al. [30] combined NAS with a trainable dynamic routing mechanism that generates data-dependent processing paths at run time. However, by incorporating the computation cost to the loss function, this approach lacks flexibility for customising deployment in applications with varying requirements or across heterogeneous devices, without retraining. Closer to our work, Layer Cascade (LC) [29] studies early-stopping for segmentation. This approach treats segmentation as a vast group of independent classification tasks, where each pixel propagates to the next exit only if the latest prediction does not surpass a confidence threshold. Nonetheless, due to different per-pixel paths, this scheme leads to heavily unstructured computations, for which existing BLAS libraries cannot achieve realistic speedups [63]. Moreover, LC constitutes a manually-crafted architecture, heavily reliant on Inception-ResNet and is not applicable to various backbones, nor does it adapt its architecture to the capabilities of the target device.

Multi-Exit Network Training. So far, the training of multi-exit models can be categorised into: 1) End-to-end schemes jointly training both the backbone and the early exits [20, 24, 72], leading to increased accuracy in early exits, at the expense of often downgrading the accuracy deeper on or even causing divergence [20, 28]. and 2) Frozen-backbone methods which firstly train the backbone until convergence and subsequently attach and train intermediate exits individually [24, 26]. This independence of the backbone from the exits allows for faster training of the exits, but at an accuracy penalty due to fewer degrees of freedom in parameter tuning. In this work, we introduce a novel two-stage training scheme for MESS networks, comprising of an exit-aware backbone training step that pushes the extraction of semantically “strong” features early in the network, followed by a frozen-backbone step for fully training the early exits without compromising the final exit’s accuracy.

A complementary approach that aims to further improve the early exits’ accuracy involves knowledge distillation between exits, studied in classification [28, 47, 71] and domain adaptation [23, 27] tasks. Such schemes employ self-distillation by treating the last exit as the teacher and the

intermediate classifiers as the students, without priors about the ground truth. In contrast, our Positive Filtering Distillation (PFD) scheme takes advantage of the densely structured information in semantic segmentation, and only allows knowledge flow for pixels the teacher is correct.

MESS networks bring together benefits from all the above worlds. Our framework combines end-to-end with frozen-backbone training, hand-engineered dilated networks with automated architectural configuration search, and latency-constrained inference with confidence-based early exiting, in a holistic approach that addresses the unique challenges of detailed scene understanding models.

3. Multi-Exit Segmentation Networks

To enable efficient segmentation, the proposed framework employs a target-specific architectural configuration search to yield a customised segmentation network optimised for the platform at hand. We call the resulting model a MESS network, with an instance depicted in Fig. 1. Yielding a MESS network involves three stages: i) starting from a backbone segmentation CNN and attaching several early exits (i.e. segmentation heads) along its depth (Sec. 3.1), ii) training them together with the backbone (Sec. 3.3) and iii) tailoring the newly defined overprovisioned network – with exits of varying architectural configuration (Sec. 3.2), accuracy and computational overhead – to application-specific requirements and the target platform (Sec. 3.4.1). Upon deployment, our framework can optimise for varying inference settings, ranging from extracting efficient sub-models satisfying particular constraints to progressive refinement of the result and confidence-based exiting (Sec. 3.4.2). Across all settings, MESS networks save computations by circumventing deeper parts of the network.

3.1. Backbone Initialisation & Exit Placement

As a first step, a CNN backbone is provided. Typical semantic segmentation CNNs try to prevent the loss of spatial information that inherently occurs in classification, without reducing the receptive field on the output pixels. For example, Dilated Residual Networks [67] allow up to $8\times$ spatial reduction in the feature maps, and replace any further traditional downsampling with a doubling in dilation rate in convolution operations. We adopt a similar assumption for the backbones used to generate MESS networks.

This approach, however, increases the feature resolution in deeper layers, which usually integrate a higher number of channels. As a result, typical CNN architectures for segmentation contain workload-heavier layers deeper on, leading to an unbalanced distribution of computational demands and an increase in the overall workload. This fact further motivates the need for early-exiting in order to eliminate unnecessary computation and save on performance.

As a next step, the provided backbone is benchmarked¹.

¹Per layer FLOPs workload, #parameters or latency on target device.

Based on the results of this analysis, N candidate exit points are identified. For simplicity, exit points are restricted to be at the output of individual network blocks b_k , following an approximately equidistant² workload distribution. This way, instead of searching between similar exit placements, we maximise the distance between one another and improve our search efficiency. An example of the described analysis on DRN-50³ backbone is presented in the Appendix.

3.2. Early-Exit Architecture

Early-exiting in DNNs faces the defiance of limited receptive field and weak semantics in shallow exits. We address these challenges in a two-fold manner: i) by pushing the extraction of semantically strong features to shallower layers of the backbone during training (Sec. 3.3) and ii) by introducing a carefully designed architectural configuration space for each exit based on its position in the backbone, which is explored to yield a MESS instance, tailored to the latency and accuracy constraints (Sec. 3.4.1).

Architectural Configuration Space. Overall, the configuration space for each exit head (Fig. 2) is shaped as:

1. Channel Reduction Module: $\mathcal{O}_{\text{crm}} = \{/1, /2, /4, /8\} \mapsto \{0, 1, 2, 3\}$
2. Extra Trainable Blocks: $\mathcal{O}_{\text{\#blocks}} = \{0, 1, 2, 3\}$
3. Rapid Dilation Increase: $\mathcal{O}_{\text{dil}} = \{\text{False}, \text{True}\} \mapsto \{0, 1\}$
4. Segmentation Head: $\mathcal{O}_{\text{head}} = \{\text{FCN-Head}, \text{DLB-Head}\} \mapsto \{0, 1\}$

Formally, we represent the configuration space for the i -th exit’s architecture as: $\mathcal{S}_{\text{exit}}^i = \mathcal{O}_{\text{crm}} \times \mathcal{O}_{\text{\#blocks}} \times \mathcal{O}_{\text{dil}} \times \mathcal{O}_{\text{head}}$, where \mathcal{O}_{crm} , $\mathcal{O}_{\text{\#blocks}}$, \mathcal{O}_{dil} and $\mathcal{O}_{\text{head}}$, are the sets of available options for the CRM, number of trainable blocks, rapid dilation increase and segmentation head respectively:

Channel Reduction Module (CRM). A main differentiating challenge of early-exiting in segmentation, compared to classification, is the significantly higher workload of segmentation heads, stemming from the enlarged input feature volume being processed. To reduce the overhead of each exit, instead of compromising the spatial resolution of the feature volume that is particularly important for accuracy, we focus our optimisation efforts on the channel dimension. In this direction, the proposed configuration space includes the optional addition of a lightweight CRM, comprising a 1×1 convolutional layer that rapidly reduces the number of channels fed to the segmentation head by a tunable factor.

Extra Trainable Blocks. Classification-centric approaches address feature extraction challenges of early classifiers by incorporating additional layers in each exit [52]. Again, due to the enlarged volume of feature maps in segmentation networks, naively introducing vanilla-sized layers may result to a surge in the exit’s workload overhead, defeating the purpose of early-exiting. In MESS networks, we expose this as a configurable option that can be employed to remedy weak semantics in shallow exits, while we carefully append such

²Every $1/N$ -th of the total backbone’s FLOPs.

³Dilated Residual Network [67] based on ResNet-50.

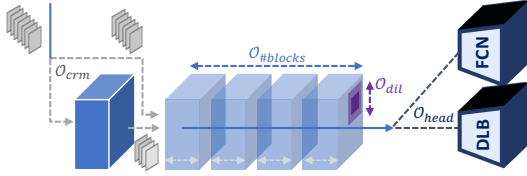


Figure 2: Parametrisation of MESS exit architecture.

layers after the CRM in order to take advantage of the computational efficiency of the reduced feature-volume width.

Rapid Dilation Increase. To address the limited receptive field of shallow exits, apart from supporting the addition of dedicated trainable layers in each exit, our framework allows the dilation rate of these layers to be rapidly increased.

Segmentation Head. Currently, the proposed framework supports two types of segmentation head architectures: i) Fully Convolutional Network-based Head (FCN-Head) [37] and ii) DeepLabV3-based Head (DLB-Head) [6, 7]. The former provides a simple and effective mechanism for upsampling the feature volume through de-convolution [44] and predicting a per-pixel probability distribution across all candidate classes. The latter incorporates Atrous Spatial Pyramid Pooling (ASPP) comprising parallel convolutions of different dilation rates in order to incorporate multi-scale contextual information to its predictions.

Notably, the majority of related work employ a uniform architecture for all exits for the sake of simplicity [20, 24, 72, 26]. However, as demonstrated in Sec. 4, different exit depths pose their own challenges, with shallow exits benefiting the most from numerous lightweight layers, whereas deeper exits favour channel-rich exit architectures. Our framework favours customisation, enabling the efficient search for a model with tailored architecture at each exit, through a two-stage training scheme (Sec. 3.3).

3.3. Training Scheme

Having the network architecture set, we move to the training methodology of our framework, comprising a two-stage pipeline enhanced with positive filtering distillation.

3.3.1 Two-Stage MESS Training

As aforementioned, early-exit networks are typically either trained end-to-end or in a frozen-backbone manner. However, both can lead to suboptimal accuracy results. For this reason, we combine the best of both worlds by proposing a novel two-stage training scheme.

Stage 1 (end-to-end). In the exit-aware pre-training stage, bare FCN-Heads⁴ are attached to all candidate exit points, generating an intermediate “super-model”. The network is trained end-to-end, updating the weights of the backbone and a single early exit at each iteration, with the remainder of the exits being dropped-out in a round-robin fashion (Eq. (1), referred to as exit-dropout loss). Formally, we denote the segmentation predictions after softmax for

⁴The selection of FCN vs. DLB heads here is for speed and guidance purposes of the coarse training step. Selected heads are refined in Stage 2.

each early exit by $\mathbf{y}_i \in [0, 1]^{R \times C \times M}$ where R and C are the output’s number of rows and columns, respectively, and M the number of classes. Given the ground-truth labels $\hat{\mathbf{y}} \in \{0, 1, \dots, M-1\}^{R \times C}$, the loss function for the proposed exit-aware pre-training stage is formulated as:

$$\mathcal{L}_{\text{pretrain}}^{\text{batch}(j)} = \sum_{i=1}^{N-1} \langle j \bmod i = 0 \rangle \cdot \mathcal{L}_{\text{CE}}(\mathbf{y}_i, \hat{\mathbf{y}}) + \mathcal{L}_{\text{CE}}(\mathbf{y}_N, \hat{\mathbf{y}}) \quad (1)$$

Although after this stage the early exits are not fully trained, their contribution to the loss pushes the backbone to extract semantically stronger features even at shallow layers.

Stage 2 (frozen-backbone). At this stage, the backbone and final exit are kept frozen (i.e. weights are not updated). All candidate early-exit architectures in $\mathcal{S}_{\text{exit}}^i$ (Sec. 3.2) are attached across all candidate exit-points $i \in \{1, 2, \dots, N\}$ and trained individually, taking advantage of the strong semantics extracted by the backbone. Most importantly, keeping the backbone unchanged allows different exit architectures to be trained without interference, and interchanged at deployment time in a plug-and-play manner, offering enormous flexibility for customisation (Sec. 3.4.1).

3.3.2 Positive Filtering Distillation

In the last stage of our training process, we further exploit the joint potential of knowledge distillation and early-exit networks for semantic segmentation. In prior self-distillation works for multi-exit networks, the backbone’s final output is used as the teacher for earlier classifiers [71], whose loss function typically combines ground-truth and distillation-specific terms [47, 38]. To further exploit what information is backpropagated from the pre-trained final exit, we propose Positive Filtering Distillation (PFD), a technique that selectively controls the flow of information to earlier exits using only signals from samples about which the last exit is correct. Our hypothesis is that early exit heads can become stronger feature extractors by incorporating signals of easy samples from the last exit, and avoiding the confusion of trying to mimic contradicting references.

Driven by the fact that segmentation outputs are dense, the proposed distillation scheme evaluates the difficulty of each pixel in the input sample with respect to the correctness of the teacher’s prediction (i.e. final output). Subsequently, we filter the stronger (higher entropy) ground-truth reference signal fed to early exits, allowing only information for “easy” pixels to pass through. Thus, we concentrate the training efforts and the learning capacity of each exit to “easier” pixels, by avoiding the pollution of the training algorithm with noisy gradients from contradicting loss terms.

Formally, we express the i -th exit’s tensor of predicted classes for each pixel $\mathbf{p} = (r, c)$ with $r \in [1, R]$ and $c \in [1, C]$ as $\hat{\mathbf{y}}_i \in \{0, 1, \dots, M-1\}^{R \times C}$ where $(\hat{\mathbf{y}}_i)_{\mathbf{p}} = \arg \max (\mathbf{y}_i)_{\mathbf{p}}$ in $\{0, 1, \dots, M-1\}$. Given the corresponding output of the final exit $\hat{\mathbf{y}}_N$, the ground-truth labels $\hat{\mathbf{y}} \in \{0, 1, \dots, M-1\}^{R \times C}$ and a hyperparameter α , we employ the loss function of Eq. (2) for the frozen-backbone stage of our training scheme:

$$\mathcal{L}_{\text{PFD}} = \sum_{i=1}^N \alpha \cdot \mathcal{L}_{\text{KL}}(\mathbf{y}_i, \mathbf{y}_N) + (1-\alpha) \cdot \mathbb{I}(\hat{\mathbf{y}}_N, \hat{\mathbf{y}}) \mathcal{L}_{\text{CE}}(\mathbf{y}_i, \hat{\mathbf{y}}) \quad (2)$$

where \mathcal{L}_{CE} and \mathcal{L}_{KL} denote the cross-entropy loss and KL divergence respectively, and \mathbb{I} the indicator function.

3.4. Deployment-time Parametrisation

Having trained the overprovisioned network comprising all candidate exit architectures, MESS instances can be derived for the use-case at hand by exhaustive architectural search, reflecting on the capabilities of the target device, the intricacy of the inputs and the required accuracy or latency.

Inference Settings. To satisfy performance needs under each device, and application-specific constraints, MESS networks support different inference settings: i) budgeted inference, in which workload-lighter sub-models up to a specific exit are extracted to enable deployment on heterogeneous platforms with diverse computational capabilities, ii) anytime inference, in which every sample goes through exits sequentially, initially providing a rapid approximation of the output and progressively refining it through deeper exits until a deadline is met, adjusting its computation depth at runtime according to the availability of resources on the target platform, or iii) input-dependent inference, where each sample dynamically follows a different computation path according to its difficulty, as captured by the confidence of each exit’s prediction (Sec. 3.4.2).

Configuration Search. Our framework tailors MESS networks for each of these settings, through an automated search of the configuration space. Concretely, we search for the number, position and architecture of early exits, along with the exit policy for the input-dependent inference case.

3.4.1 Number, Placement & Configuration of Exits

The proposed methodology contemplates all trained exit architectures and exhaustively creates different configurations, trading for example a workload-heavier shallow exit with a more lightweight deeper exit. The search strategy considers the target inference setting, along with user-specified requirements in workload, latency and accuracy, which can be expressed as a combination of hard constraints and optimisation objectives. As a result, the number and placement of exits and the architecture of each individual exit of the resulting MESS instance are jointly optimised.

Given the exit-architecture search space $\mathcal{S}_{\text{exit}}^i$ (Sec. 3.2), we define the configuration space of a MESS network as:

$$\mathcal{S} = (\mathcal{S}_{\text{exit}}^1 + 1) \times (\mathcal{S}_{\text{exit}}^2 + 1) \times \dots \times (\mathcal{S}_{\text{exit}}^N + 1) \quad (3)$$

where the extra term accounts for a “None” option for each of the exit positions. Under this formulation, the framework can minimise workload/latency (expressed as cost^5), given an *accuracy* constraint th_{acc} :

$$s^* = \arg \min_{s \in \mathcal{S}} \{\text{cost}(s) \mid \text{acc}(s) \geq th_{\text{acc}}\} \quad (4)$$

⁵Formally expressed for each inference setting in the Appendix.

or optimise for *accuracy*, given a *cost* constraint th_{cost} :

$$s^* = \arg \max_{s \in \mathcal{S}} \{\text{acc}(s) \mid \text{cost}(s) \leq th_{\text{cost}}\} \quad (5)$$

Most importantly, our two-stage training scheme of Sec. 3.3.1 allows all trained exits to be interchangeably attached to the same backbone for inference. This allows for an extremely efficient search of an overly complex space, avoiding the excessive search times of NAS approaches [4]. Additionally, MESS networks can be customised for different requirements without the need for re-training, while the exhaustive enumeration of our search guarantees the optimality of the selected design point.

3.4.2 Input-Dependent Exit Policy

Early-exit Criterion. Driven by the fact that not all inputs pose the same prediction difficulty, adaptive inference has been widely studied in image classification (Sec. 2). In this setting, each input sample goes through the selected early exits sequentially. After a prediction is produced from an exit, a mechanism to calculate an image-level confidence (as a metric of predicting difficulty) is used to determine whether inference should continue to the next exit or not.

This technique remains highly unexplored in dense prediction problems, such as semantic segmentation. In [29] each pixel in an image is treated as an independent classification task, exiting early if its prediction confidence in an exit is high, thus yielding irregular computation paths. In contrast, our approach treats the segmentation of each image as a single task, aiming to drive each sample through a uniform computation route. To this end, we fill a gap in literature by introducing a novel mechanism to quantify the overall confidence in semantic segmentation predictions.

Confidence-tuning for MESS Networks. Starting from a per-pixel confidence map, calculated based on the probability distribution across classes of each pixel $\mathbf{c}^{\text{map}} = f_c(\mathbf{y}) \in [0, 1]^{R \times C}$ (where f_c is usually $\text{top1}(\cdot)$ [20] or $\text{entropy}(\cdot)$ [8]), we introduce a mechanism to reduce these every-pixel confidence values to a single (per-image) confidence value. The proposed metric considers the percentage of pixels with high prediction confidence (above a tunable threshold th_i^{pix}) in the dense output of an exit \mathbf{y}_i :

$$c_i^{\text{ovrl}} = \frac{1}{RC} \sum_{r=1}^R \sum_{c=1}^C \mathbb{I}(c_{r,c}^{\text{map}}(\mathbf{y}_i) \geq th_i^{\text{pix}}) \quad (6)$$

Moreover, it has been observed that due to the progressive downsampling of the feature volume in CNNs, some spatial information is lost. As a result, semantic predictions near object edges are naturally under-confident [54]. Driven by this observation, we enhance our proposed metric to account for these expected low-confidence pixel-predictions. Initially, we conduct edge detection on the semantic masks, followed by an erosion filter with kernel equal to the feature volume spatial downsampling rate ($8\times$), in order to compute a semantic-edge map \mathcal{M} :

$$\mathcal{M} = \text{erode}(\text{cannyEdge}(\hat{\mathbf{y}}_i), 8) \quad (7)$$

Table 1: Per-exit accuracy for different training schemes on DRN-50. The first two groups of rows illustrate different end-to-end trainings employing different losses. The last group represents different training schemes, using candidates of the first group as initialisations.

Baseline	Training		Init.	Loss	Mean IoU: Exit(Backbone Workload %)*						
	- DRN-50 -				$\mathcal{E}_1(\sim 20\%)$	$\mathcal{E}_2(\sim 30\%)$	$\mathcal{E}_3(\sim 40\%)$	$\mathcal{E}_4(\sim 60\%)$	$\mathcal{E}_5(\sim 80\%)$	$\mathcal{E}_6(100\%)$	
Initialisation Variant	(i)	End-to-End	ImageNet	$CE(\mathcal{E}_6)$	-	-	-	-	-	-	59.02%
Initialisation Variant	(ii)	End-to-End	ImageNet	$CE(\mathcal{E}_3)+CE(\mathcal{E}_6)$	-	-	49.82	-	-	-	59.64%
Initialisation Variant	(iii)	End-to-End	ImageNet	$CE(\mathcal{E}_1)+CE(\mathcal{E}_6)$	34.94%	-	-	-	-	-	58.25%
Initialisation (Ours)	(iv)	End-to-End	ImageNet	Eq. (1) (Ours)	28.21%	39.61%	47.13%	50.81%	56.11%	-	59.90%
E2E SOTA [20, 52]	(v)	End-to-End	ImageNet	$CE(\mathcal{E}_1)+\dots+CE(\mathcal{E}_6)$	29.02%	40.67%	48.64%	51.69%	55.34%	-	58.33%
Frozen SOTA [24, 26]	(vi)	Frozen	(i)	$CE(\mathcal{E}_1), \dots, CE(\mathcal{E}_5)$	23.94%	31.50%	38.24%	44.73%	54.32%	-	59.02%
Frozen Ablated Variant	(vii)	Frozen	(ii)	$CE(\mathcal{E}_1), \dots, CE(\mathcal{E}_5)$	27.79%	39.11%	49.96%	51.84%	56.88%	-	59.64%
Frozen Ablated Variant	(viii)	Frozen	(iii)	$CE(\mathcal{E}_1), \dots, CE(\mathcal{E}_5)$	35.15%	38.76%	42.60%	46.77%	54.83%	-	58.25%
Ours	(ix)	Frozen	(iv)	$CE(\mathcal{E}_1), \dots, CE(\mathcal{E}_5)$	32.40%	43.34%	50.81%	53.73%	57.9%	-	59.90%

* Experiments repeated 3 times. The sample stdev in mean IoU is at most ± 0.09 in all cases.

Finally, we apply a median-based smoothing on the confidence values of pixels lying on the semantic edges:

$$\widehat{c}_{r,c}^{\text{map}}(y_i) = \begin{cases} \text{median}(c_{w_r, w_c}^{\text{map}}(y_i)) & \text{if } \mathcal{M}_{r,c} = 1 \\ c_{r,c}^{\text{map}}(y_i) & \text{otherwise} \end{cases} \quad (8)$$

where $w_l = \{l-W, \dots, l+W\}$ and W is a tunable window size.

At inference time, each sample is sequentially processed by the selected early exits. For each prediction y_i , the proposed metric c_i^{ovrl} is calculated, and a tunable confidence threshold (exposed to the search space as exit policy) determines whether the sample will exit early ($c_i^{\text{ovrl}} \geq th_i$) or be processed further by subsequent backbone layers/exits.

4. Evaluation

4.1. Experimental Setup⁶

Models & Datasets. We apply the proposed methodology on top of DRN-50 [67], DeepLabV3 [6] and MNetV2 [49] segmentation CNNs, using ResNet50 [17] and MobileNetV2 [49] backbones, representing high-end and edge use-cases respectively. We train all backbones on MS COCO [33] and fine-tune early exits on MS COCO and PASCAL VOC (augmented from [16]) independently.

Development & Deployment Setup. MESS networks are implemented on PyTorch (v1.6.0), building on top of torchvision (v0.6.0). At inference time, we deploy MESS network instances on both a high-end (Nvidia GTX1080Ti-equipped desktop; 400W TDP) and an edge (Nvidia Jetson Xavier AGX; 30W TDP) platform.

Baselines. To assess our work’s performance against the state-of-the-art (SOTA), we compare with the following baselines: 1) **E2E SOTA** [20, 52]; 2) **Frozen SOTA** [24, 26]; 3) **SelfDistill** [72, 47, 71]; 4) **DRN** [67]; 5) **DLBV3** [67, 7]; 6) **segMBNetV2** [49]; and 7) **LC** [29]. Details on each baseline can be found in the Appendix.

4.2. MESS Networks Training

4.2.1 Exit-Aware Pre-training

Initially, we demonstrate the effectiveness of the proposed exit-aware pre-training scheme. We compare the accuracy of models with uniform exit configuration across all candidate exits points, trained using different strategies. Table 1 summarises the results of this comparison on a ResNet50-based DRN backbone (DRN-50) with $N = 6$. The top cluster (rows (i)-(iv)) provides alternative initialisation schemes

⁶More extensively discussed in the Appendix.

for the network, each using a different loss function and integrating different exits. These serve as alternatives to the end-to-end pre-training step (stage 1, defined in Sec. 3.3.1).

By adding an early exit into the loss function, we essentially aim to push the extraction of semantically strong features towards shallow parts of the network. Results from different initialisations show that adding a single exit under end-to-end training can even boost the accuracy of the final segmentation prediction (row (ii)). Similar to its usage in GoogLeNet [51], we fathom that the extra signal midway through the network acts both as a regulariser and as an extra backpropagation source, reducing the potential effect of vanishing gradients. However, this effect quickly fades when exits are attached at very early layers (row (iii)) or when more exits are attached and trained jointly. This is depicted in **E2E SOTA** (row (v)), which represents the end-to-end training scheme of [20, 52]. Both of these training approaches can lead to degraded accuracy of the final output, probably attributed to contradicting signals between the early and the late classifiers and to the larger losses of the early results, which dominate the loss function [3]. Therefore, we propose an exit-dropout loss that only trains the early exits one-by-one in an alternating fashion, yielding the highest accuracy on the final exit (row (iv)).

The bottom cluster of rows lists the same setups as before, but after the second stage of training is applied, as defined in Sec. 3.3.1. For example, **Frozen SOTA** (row (vi)) represents the case where the early exits are trained when attached to a frozen pre-trained vanilla backbone, similar to [24, 26]. A key takeaway is that jointly pre-training with at least one early exit can partly benefit adjacent exit heads in the second stage (rows (vii)-(viii) vs. (vi)). However, this effect is largely angled towards the particular exit that was selected during the pre-training and may come at a cost for the deepest classifier. In contrast, our proposed exit-aware initialisation scheme (row (ix)) yields consistently high accuracy results across all exits, without hurting the final exit.

Indicatively, our exit-dropout loss helps the resulting exits to achieve an accuracy gain of up to 12.57 percentage points (pp) compared to a traditionally pre-trained segmentation network (row (i)), and up to 3.38 pp compared to an end-to-end trained model (row (v)), which also suffers a 1.57 pp drop in the accuracy of the final exit.

Table 2: Positive Filtering Distillation ablation (mIoU).

Baseline	Loss	DRN-50			MobileNetV2		
		\mathcal{E}_1	\mathcal{E}_2	\mathcal{E}_3	\mathcal{E}_1	\mathcal{E}_2	\mathcal{E}_3
E2E SOTA [20, 52]	CE	49.96%	55.40%	58.96%	31.56%	41.57%	51.59%
KD [18]	KD	50.66%	55.91%	58.84%	32.08%	41.96%	51.58%
SelfDistill [72, 47, 71]	CE+KD	50.33%	55.67%	59.08%	31.04%	41.93%	51.66%
Ours (§3.3.2)	PFD	51.02%	56.21%	59.36%	33.36%	42.95%	52.20%

CE=Cross-entropy, KD=Knowledge Distillation, PFD=Positive Filtering Distillation

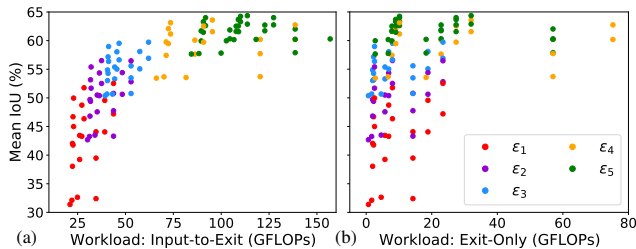


Figure 3: Workload-accuracy trade-off in design points with varying architectural configuration and exit position. Capturing: (a) input-to-exit workload examined in budgeted inference, (b) solely the overhead of each exit used for anytime inference.

4.2.2 Positive Filtering Distillation

Here, we quantify the benefits of our Positive Filtering Distillation (PFD) scheme for the second stage (frozen-backbone) of our training methodology. To this end, we compare against **E2E SOTA** that utilises cross-entropy loss (CE), the traditional knowledge distillation (KD) approach [18], and **SelfDistill** employing a combined loss (CE+KD). Table 2 summarises our results on a representative exit-architecture, on both DRN-50 and MobileNetV2.

Our proposed loss consistently yields higher accuracy across all cases, achieving up to 1.8, 1.28 and 2.32 pp accuracy gains over **E2E SOTA**, **KD** and **SelfDistill**, respectively. This accuracy boost is more salient on shallow exits, whereas a narrower improvement is obtained in deeper exits, where the accuracy gap to the final exit is natively bridged.

4.3. Inference Performance Evaluation

In this section, we showcase the effectiveness and flexibility of the proposed train-once, deploy-everywhere approach for semantic segmentation, under varying deployment scenarios and workload/accuracy constraints. As mentioned in Sec. 3.4, there are three inference settings in MESS networks: i) budgeted inference, ii) anytime inference and iii) input-dependent inference, for which we can optimise separately. For this reason, we deploy our search to find the best early-exit architecture for the respective use-case. We showcase the performance of optimised MESS networks, under such scenarios below.

4.3.1 Budgeted and Anytime Inference

Fig. 3 depicts the underlying workload-accuracy relationship across the architectural configuration space for DRN-50 backbone with FCN exits. Different points represent different architectures, colour-coded by their placement in the network. To guide our conclusions on the best designs across the inference modes, we complement our experiments with measurements from two-exit networks, meeting

Table 3: Workload and accuracy for DRN-50 with one early exit for different inference schemes. (Requirement of 50% mean IoU)

Inference	Workload (GFLOPs)			Mean IoU	
	Overhead	$\mathcal{E}_{\text{early}}$	$\mathcal{E}_{\text{final}}$	$\mathcal{E}_{\text{early}}$	$\mathcal{E}_{\text{final}}$
(i) Final-Only	-	-	138.63	-	59.90%
(ii) Budgeted	8.01	28.34	-	51.76%	-
(iii) Anytime	0.69	39.32	139.33	50.37%	59.90%
(iv) Input-Dep.	2.54	(\mathcal{E}_{sel} : 23.02)	(\mathcal{E}_{sel} : 50.03%)		

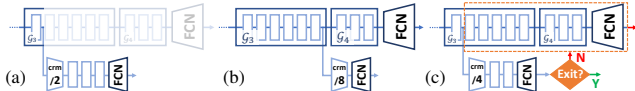


Figure 4: Selected design points for: (a) budgeted, (b) anytime and (c) input-dependent inference, with the same accuracy target.

a 50% mean IoU requirement, presented in Table 3.

In budgeted inference, we search for a submodel that can fit on the device and execute within a given latency/memory/accuracy target. Our method is able to provide the most efficient MESS network configuration, tailored to the requirements of the underlying application and device. This optimality gets translated in Fig. 3a, showcasing the cost-accuracy trade-off from the input until the respective early exit of the network, in the presence of candidate design points along the Pareto front of the search space. In this setting, our search tends to favour designs with powerful exit architectures, consisting of multiple trainable layers, and mounted earlier in the network (Fig. 4a).

For the case of anytime inference, we treat a given deadline as a cut-off point of computation. When this deadline is met, we simply take the last output of the early exit network available – or use this as a placeholder result to be asynchronously refined until the result is actually used. In this paradigm, however, there is an inherent trade-off. On the one hand, denser early exits provide more frequent “check-points”. On the other hand, each added head is essentially a computational overhead when not explicitly used. To control this trade-off, our method also considers the additional computational cost of each exit, when populating the MESS network architecture (Fig. 3b). Contrary to budgeted inference, in this setting our search produces heads with extremely lightweight architecture, sacrificing flexibility for reduced computational overhead, mounted deeper in the network (Fig. 4b). Table 3 showcases that, for anytime inference, our search yields an exit architecture with 11.6× less computational requirements compared to budgeted inference, under the same accuracy constraint.

4.3.2 Input-Dependent Inference

In the input-dependent inference setting, each input sample propagates through the MESS network at hand and until the model yields a prediction (\mathcal{E}_{sel}) about which it is confident enough (Eq. (6)). In this section, we instantiate MESS networks under this setting and evaluate our novel confidence metric for dense scene understanding (Sec. 3.4.2).

Confidence Evaluation. Different confidence-based metrics have been proposed for early-exiting. In the realm of

Table 4: End-to-end evaluation of MESS network designs

Baseline	Backbone*	Head	Search Targets	Results: MS-COCO			Results: Pascal-VOC			
				Error	GFLOPs	mIoU	GFLOPs	Latency [†]	mIoU	GFLOPs
DRN [67]	(i)	ResNet50	FCN	–Baseline–	59.02%	138.63	39.96ms	72.23%	138.63	39.93ms
Ours	(ii)	ResNet50	FCN	min $\leq 1\times$	64.35%	113.65	37.53ms	79.09%	113.65	37.59ms
Ours	(iii)	ResNet50	FCN	$\leq 0.1\%$ min	58.91%	41.17	17.92ms	72.16%	44.81	18.63ms
Ours	(iv)	ResNet50	FCN	$\leq 1\%$ min	58.12%	34.53	15.11ms	71.29%	38.51	16.80ms
DLBV3 [6, 7]	(v)	ResNet50	DLB	–Baseline–	64.94%	163.86	59.05ms	80.27%	163.86	59.06ms
Ours	(vi)	ResNet50	DLB	min $\leq 1\times$	65.52%	124.10	43.29ms	80.60%	142.38	43.29ms
Ours	(vii)	ResNet50	DLB	$\leq 0.1\%$ min	64.86%	69.84	24.81ms	80.18%	85.61	31.54ms
Ours	(viii)	ResNet50	DLB	$\leq 1\%$ min	64.03%	57.01	20.83ms	79.40%	74.20	27.63ms
segMBNetV2 [49]	(ix)	MobileNetV2	FCN	–Baseline–	54.24%	8.78	67.04ms	69.68%	8.78	67.06ms
Ours	(x)	MobileNetV2	FCN	min $\leq 1\times$	57.49%	8.10	56.05ms	74.22%	8.10	56.09ms
Ours	(xi)	MobileNetV2	FCN	$\leq 0.1\%$ min	54.18%	4.05	40.97ms	69.61%	3.92	32.79ms
Ours	(xii)	MobileNetV2	FCN	$\leq 1\%$ min	53.24%	3.48	38.83ms	68.80%	3.60	31.40ms

*Dilated network [67] based on backbone CNN. [†]Measured on: GTX for ResNet50 and AGX for MobileNetV2 backbone.

classification, these revolve around comparing the entropy [52] or top1 [20] result of the respective exit’s softmax to a threshold. On top of this, segmentation presents the problem of dense predictions. As such, we can either naively adapt these widely-employed classification-based metrics to segmentation by averaging per-pixel confidences for an image or apply our proposed custom metric presented in Sec. 3.4.2. The Cartesian product of these approaches defines four baselines depicted in Fig. 5, where we benchmark the effectiveness of our proposed exit scheme against other policies on a DRN-50-based MESS network with two exits. By selecting different threshold values for the exit policy, even the simplest (2-exit) configuration of input-dependent MESS network (Fig. 4c) provides a fine-grained trade-off between workload and accuracy. Exploiting this trade-off, we observe that input-dependent inference (Table 3; row (iv)) offers the highest computational efficiency under the same 50% mean IoU accuracy constraint.

Furthermore, it can be observed that the proposed image-level confidence metric, applied on top of both top1 probability and entropy-based pixel-level confidence estimators, provides a consistently better accuracy-efficiency trade-off compared to the corresponding averaging counterparts. Specifically, experiments with various architectural configurations showcase a gain of up to 6.34 pp (1.17 pp on average) across the spectrum of thresholding values.

4.3.3 Comparison with SOTA Segmentation Networks

Single-exit Segmentation Solutions. Here, we continue with input-dependent inference and apply our MESS framework on single-exit alternatives from the literature, namely **DRN**, **DLBV3** and **segMBNetV2**. Table 4 lists the achieved results for MESS instances optimised for varying use-cases (framed as speed/accuracy requirements fed to our configuration search), as well as the original models.

For a DRN-50 backbone with FCN head on MS COCO, we observe that a latency-optimised MESS instance with no accuracy drop (row (iii)) can achieve a workload reduction of up to 3.36 \times , translating to a latency speedup of 2.23 \times over the single-exit **DRN**. This improvement is amplified to 4.01 \times in workload (2.65 \times in latency) for cases that can tolerate a controlled accuracy degradation of ≤ 1 pp (row (iv)). Additionally, a MESS instance optimised for accuracy under the same workload budget as **DRN**, achieves an mIoU

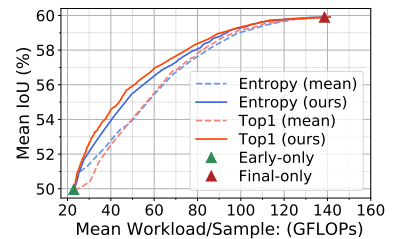


Figure 5: Comparison of different early-exit policies/metrics on a DRN-50-based MESS instance with 2 exits.

gain of 5.33 pp with 1.22 \times fewer GFLOPs (row (ii)).

Similar results are obtained against **DLBV3**, as well as when targeting the PASCAL VOC dataset. Moreover, the performance gains are consistent against **segMBNetV2** (rows (ix)-(xii)), which forms an inherently efficient segmentation design, with 15.7 \times smaller workload than DRN-50. This demonstrates the model-agnostic nature of our framework, yielding complementary gains by exploiting the dimension of input-dependent inference.

Multi-exit Segmentation Solutions. Next, we compare the accuracy and performance of MESS networks against Deep Layer Cascade (**LC**) [29] networks, a SOTA work that proposes per-pixel propagation in early-exit segmentation networks. Due to their heavily unstructured computation, standard BLAS libraries cannot realise the true benefits of this approach and, therefore, we apply **LC**’s pixel-level exit policy on numerous MESS configurations, and compare with our image-level policy analytically.

By using SOTA approaches in semantic segmentation, such as larger dilation rates or DeepLab’s ASPP, the gains of **LC** rapidly fade away, as for each pixel that propagates deeper on, a substantial feature volume needs to be precomputed. Concretely, by using the FCN-head, a substantial 45% of the feature volume at the output of the first exit falls within the receptive field of a single pixel in the final output, reaching 100% for DLB-Head. As a result, we observe no workload reduction for **LC** for the 2-exit network of Table 3 (row (iv)) and heavily dissipated gains of 1.13 \times for the 3-exit network of Table 4 (row (iii)), against the corresponding baselines of row (i). In contrast, the respective MESS instances achieve a workload reduction of 6.02 \times and 3.36 \times .

5. Conclusion

We have proposed MESS networks, multi-exit models that perform efficient semantic segmentation, applicable on top of state-of-the-art CNN approaches without sacrificing accuracy. This is achieved by introducing novel training and early-exiting techniques, tailored for MESS networks. Post-training, our framework can customise the MESS network by searching for the optimal multi-exit configuration (number, placement and architecture of exits) according to the target platform, pushing the limits of efficient deployment.

Further quantitative & qualitative results discussed in the Appendix.

References

- [1] Mario Almeida, Stefanos Laskaridis, Ilias Leontiadis, Stylianos I. Venieris, and Nicholas D. Lane. EmBench: Quantifying Performance Variations of Deep Neural Networks Across Modern Commodity Devices. In *The 3rd International Workshop on Deep Learning for Mobile Systems and Applications (EMDL)*, 2019. [1](#)
- [2] Vijay Badrinarayanan, Alex Kendall, and Roberto Cipolla. SegNet: A Deep Convolutional Encoder-Decoder Architecture for Image Segmentation. *IEEE Transactions on Pattern Analysis and Machine Intelligence (TPAMI)*, 39(12):2481–2495, 2017. [2](#)
- [3] Tolga Bolukbasi, Joseph Wang, Ofer Dekel, and Venkatesh Saligrama. Adaptive Neural Networks for Efficient Inference. In *International Conference on Machine Learning (ICML)*, pages 527–536, 2017. [2](#), [6](#)
- [4] Liang-Chieh Chen, Maxwell Collins, Yukun Zhu, George Papandreou, Barret Zoph, Florian Schroff, Hartwig Adam, and Jon Shlens. Searching for efficient multi-scale architectures for dense image prediction. In *Advances in Neural Information Processing Systems (NeurIPS)*, pages 8699–8710, 2018. [5](#), [13](#)
- [5] Liang-Chieh Chen, George Papandreou, Iasonas Kokkinos, Kevin Murphy, and Alan L Yuille. DeepLab: Semantic Image Segmentation with Deep Convolutional Nets, Atrous Convolution, and Fully Connected CRFs. *IEEE Transactions on Pattern Analysis and Machine Intelligence (TPAMI)*, 40(4):834–848, 2017. [2](#)
- [6] Liang-Chieh Chen, George Papandreou, Florian Schroff, and Hartwig Adam. Rethinking Atrous Convolution for Semantic Image Segmentation. *arXiv preprint arXiv:1706.05587*, 2017. [1](#), [4](#), [6](#), [8](#), [12](#)
- [7] Liang-Chieh Chen, Yukun Zhu, George Papandreou, Florian Schroff, and Hartwig Adam. Encoder-Decoder with Atrous Separable Convolution for Semantic Image Segmentation. In *European Conference on Computer Vision (ECCV)*, pages 801–818, 2018. [4](#), [6](#), [8](#), [12](#)
- [8] Feiyang Cheng, Hong Zhang, Ding Yuan, and Mingui Sun. Leveraging semantic segmentation with learning-based confidence measure. *Neurocomputing*, 329:21–31, 2019. [5](#)
- [9] Jia Deng, Wei Dong, Richard Socher, Li-Jia Li, Kai Li, and Li Fei-Fei. ImageNet: A Large-Scale Hierarchical Image Database. In *IEEE Conference on Computer Vision and Pattern Recognition (CVPR)*, pages 248–255, 2009. [12](#)
- [10] Mark Everingham, Luc Van Gool, Christopher KI Williams, John Winn, and Andrew Zisserman. The Pascal Visual Object Classes (VOC) Challenge. *International Journal of Computer Vision (IJCV)*, 88(2):303–338, 2010. [12](#)
- [11] Biyi Fang, Xiao Zeng, and Mi Zhang. NestDNN: Resource-Aware Multi-Tenant On-Device Deep Learning for Continuous Mobile Vision. In *Annual International Conference on Mobile Computing and Networking (MobiCom)*, page 115–127, 2018. [2](#)
- [12] Michael Figurnov, Maxwell D Collins, Yukun Zhu, Li Zhang, Jonathan Huang, Dmitry Vetrov, and Ruslan Salakhutdinov. Spatially Adaptive Computation Time for Residual Networks. In *IEEE Conference on Computer Vision and Pattern Recognition (CVPR)*, pages 1039–1048, 2017. [2](#)
- [13] Xitong Gao, Yiren Zhao, Łukasz Dudziak, Robert Mullins, and Cheng zhong Xu. Dynamic Channel Pruning: Feature Boosting and Suppression. In *International Conference on Learning Representations*, 2019. [2](#)
- [14] Golnaz Ghiasi and Charles C Fowlkes. Laplacian pyramid reconstruction and refinement for semantic segmentation. In *European Conference on Computer Vision (ECCV)*, pages 519–534. Springer, 2016. [2](#)
- [15] Swarnendu Ghosh, Nibaran Das, Ishita Das, and Ujjwal Maulik. Understanding Deep Learning Techniques for Image Segmentation. *ACM Computing Surveys (CSUR)*, 52(4):1–35, 2019. [1](#)
- [16] Bharath Hariharan, Pablo Arbeláez, Lubomir Bourdev, Subhransu Maji, and Jitendra Malik. Semantic contours from inverse detectors. In *2011 International Conference on Computer Vision*, pages 991–998. IEEE, 2011. [6](#), [12](#)
- [17] Kaiming He, Xiangyu Zhang, Shaoqing Ren, and Jian Sun. Deep Residual Learning for Image Recognition. In *IEEE Conference on Computer Vision and Pattern Recognition (CVPR)*, pages 770–778, 2016. [2](#), [6](#)
- [18] Geoffrey Hinton, Oriol Vinyals, and Jeff Dean. Distilling the Knowledge in a Neural Network. In *NeurIPS 2014 Deep Learning Workshop*, 2014. [7](#)
- [19] Weizhe Hua, Yuan Zhou, Christopher M De Sa, Zhiru Zhang, and G. Edward Suh. Channel Gating Neural Networks. In *Advances in Neural Information Processing Systems (NeurIPS)*, pages 1886–1896. 2019. [2](#)
- [20] Gao Huang, Danlu Chen, Tianhong Li, Felix Wu, Laurens van der Maaten, and Kilian Weinberger. Multi-Scale Dense Networks for Resource Efficient Image Classification. In *International Conference on Learning Representations (ICLR)*, 2018. [1](#), [2](#), [4](#), [5](#), [6](#), [7](#), [8](#), [12](#), [13](#)
- [21] Gao Huang, Zhuang Liu, Laurens Van Der Maaten, and Kilian Q Weinberger. Densely Connected Convolutional Networks. In *IEEE Conference on Computer Vision and Pattern Recognition (CVPR)*, pages 4700–4708, 2017. [2](#)
- [22] Andrey Ignatov, Radu Timofte, Andrei Kulik, Seungsoo Yang, Ke Wang, Felix Baum, Max Wu, Lirong Xu, and Luc Van Gool. AI Benchmark: All About Deep Learning on Smartphones in 2019. In *International Conference on Computer Vision (ICCV) Workshops*, 2019. [1](#)
- [23] Jinguang Jiang, Ximei Wang, Mingsheng Long, and Jianmin Wang. Resource Efficient Domain Adaptation. In *ACM International Conference on Multimedia (MM)*, 2020. [2](#)
- [24] Yigitcan Kaya, Sanghyun Hong, and Tudor Dumitras. Shallow-Deep Networks: Understanding and Mitigating Network Overthinking. In *International Conference on Machine Learning (ICML)*, pages 3301–3310, 2019. [1](#), [2](#), [4](#), [6](#), [12](#), [13](#)
- [25] Stefanos Laskaridis, Stylianos I. Venieris, Mario Almeida, Ilias Leontiadis, and Nicholas D. Lane. SPINN: Synergistic Progressive Inference of Neural Networks over Device and Cloud. In *Annual International Conference on Mobile Computing and Networking (MobiCom)*. Association for Computing Machinery, 2020. [2](#)

- [26] Stefanos Laskaridis, Stylianos I. Venieris, Hyeji Kim, and Nicholas D. Lane. HAPI: Hardware-Aware Progressive Inference. In International Conference on Computer-Aided Design (ICCAD), 2020. 2, 4, 6, 12, 13
- [27] Ilias Leontiadis, Stefanos Laskaridis, Stylianos I. Venieris, and Nicholas D. Lane. It’s Always Personal: Using Early Exits for Efficient On-Device CNN Personalisation. In Proceedings of the 22nd International Workshop on Mobile Computing Systems and Applications (HotMobile), 2021. 2
- [28] Hao Li, Hong Zhang, Xiaojuan Qi, Ruigang Yang, and Gao Huang. Improved Techniques for Training Adaptive Deep Networks. In IEEE International Conference on Computer Vision (ICCV), 2019. 2
- [29] Xiaoxiao Li, Ziwei Liu, Ping Luo, Chen Change Loy, and Xiaoou Tang. Not All Pixels Are Equal: Difficulty-aware Semantic Segmentation via Deep Layer Cascade. In IEEE Conference on Computer Vision and Pattern Recognition (CVPR), pages 3193–3202, 2017. 2, 5, 6, 8, 12
- [30] Yanwei Li, Lin Song, Yukang Chen, Zeming Li, Xiangyu Zhang, Xingang Wang, and Jian Sun. Learning Dynamic Routing for Semantic Segmentation. In IEEE/CVF Conference on Computer Vision and Pattern Recognition (CVPR), pages 8553–8562, 2020. 2, 13
- [31] Guosheng Lin, Anton Milan, Chunhua Shen, and Ian Reid. Refinenet: Multi-Path Refinement Networks for High-Resolution Semantic Segmentation. In IEEE Conference on Computer Vision and Pattern Recognition (CVPR), pages 1925–1934, 2017. 2
- [32] Ji Lin, Yongming Rao, Jiwen Lu, and Jie Zhou. Runtime Neural Pruning. In Advances in Neural Information Processing Systems (NeurIPS), pages 2181–2191, 2017. 2
- [33] Tsung-Yi Lin, Michael Maire, Serge Belongie, James Hays, Pietro Perona, Deva Ramanan, Piotr Dollár, and C Lawrence Zitnick. Microsoft COCO: Common Objects in Context. In European Conference on Computer Vision (ECCV), pages 740–755, 2014. 6
- [34] Chenxi Liu, Liang-Chieh Chen, Florian Schroff, Hartwig Adam, Wei Hua, Alan L Yuille, and Li Fei-Fei. Auto-DeepLab: Hierarchical Neural Architecture Search for Semantic Image Segmentation. In IEEE Conference on Computer Vision and Pattern Recognition (CVPR), pages 82–92, 2019. 1, 2, 13
- [35] Luyang Liu, Hongyu Li, and Marco Gruteser. Edge Assisted Real-Time Object Detection for Mobile Augmented Reality. In Annual International Conference on Mobile Computing and Networking (MobiCom), 2019. 1
- [36] Yifan Liu, Ke Chen, Chris Liu, Zengchang Qin, Zhenbo Luo, and Jingdong Wang. Structured Knowledge Distillation for Semantic Segmentation. In IEEE Conference on Computer Vision and Pattern Recognition (CVPR), pages 2604–2613, 2019. 2
- [37] Jonathan Long, Evan Shelhamer, and Trevor Darrell. Fully Convolutional Networks for Semantic Segmentation. In IEEE Conference on Computer Vision and Pattern Recognition (CVPR), pages 3431–3440, 2015. 2, 4
- [38] Yunteng Luan, Hanyu Zhao, Zhi Yang, and Yafei Dai. MSD: Multi-Self-Distillation Learning via Multi-classifiers within Deep Neural Networks. arXiv preprint arXiv:1911.09418, 2019. 4
- [39] Pauline Luc, Camille Couprie, Soumith Chintala, and Jakob Verbeek. Semantic Segmentation using Adversarial Networks. In NIPS Workshop on Adversarial Training, 2016. 2
- [40] John McCormac, Ankur Handa, Andrew Davison, and Stefan Leutenegger. SemanticFusion: Dense 3D Semantic Mapping with Convolutional Neural Networks. In 2017 IEEE International Conference on Robotics and Automation (ICRA), pages 4628–4635. IEEE, 2017. 1
- [41] Sachin Mehta, Mohammad Rastegari, Anat Caspi, Linda Shapiro, and Hannaneh Hajishirzi. ESPNet: Efficient Spatial Pyramid of Dilated Convolutions for Semantic Segmentation. In European Conference on Computer Vision (ECCV), pages 552–568, 2018. 1, 2
- [42] Vladimir Nekrasov, Hao Chen, Chunhua Shen, and Ian Reid. Fast Neural Architecture Search of Compact Semantic Segmentation Models via Auxiliary Cells. In IEEE Conference on Computer Vision and Pattern Recognition (CVPR), pages 9126–9135, 2019. 2, 13
- [43] Hyeonwoo Noh, Seunghoon Hong, and Bohyung Han. Learning Deconvolution Network for Semantic Segmentation. In IEEE International Conference on Computer Vision (ICCV), pages 1520–1528, 2015. 2
- [44] Hyeonwoo Noh, Seunghoon Hong, and Bohyung Han. Learning Deconvolution Network for Semantic Segmentation. In IEEE International Conference on Computer Vision (ICCV), 2015. 4
- [45] NVIDIA. NVIDIA Maxine - Cloud-AI Video-Streaming Platform. <https://developer.nvidia.com/maxine>, 2020. [Retrieved: June 8, 2021]. 1
- [46] Chao Peng, Xiangyu Zhang, Gang Yu, Guiming Luo, and Jian Sun. Large Kernel Matters—Improve Semantic Segmentation by Global Convolutional Network. In IEEE Conference on Computer Vision and Pattern Recognition (CVPR), pages 4353–4361, 2017. 1
- [47] Mary Phuong and Christoph H Lampert. Distillation-based Training for Multi-Exit Architectures. In IEEE International Conference on Computer Vision (ICCV), pages 1355–1364, 2019. 2, 4, 6, 7, 12
- [48] Olaf Ronneberger, Philipp Fischer, and Thomas Brox. U-Net: Convolutional Networks for Biomedical Image Segmentation. In International Conference on Medical Image Computing and Computer-Assisted Intervention, pages 234–241. Springer, 2015. 2
- [49] Mark Sandler, Andrew Howard, Menglong Zhu, Andrey Zhmoginov, and Liang-Chieh Chen. MobileNetV2: Inverted Residuals and Linear Bottlenecks. In IEEE Conference on Computer Vision and Pattern Recognition (CVPR), pages 4510–4520, 2018. 6, 8, 12, 13
- [50] Mennatullah Siam, Mostafa Gamal, Moemen Abdel-Razek, Senthil Yogamani, Martin Jagersand, and Hong Zhang. A Comparative Study of Real-Time Semantic Segmentation for Autonomous Driving. In IEEE Conference on Computer Vision and Pattern Recognition (CVPR) Workshops, 2018. 1
- [51] Christian Szegedy, Wei Liu, Yangqing Jia, Pierre Sermanet, Scott Reed, Dragomir Anguelov, Dumitru Erhan, Vincent

- Vanhoucke, and Andrew Rabinovich. Going Deeper with Convolutions. In IEEE Conference on Computer Vision and Pattern Recognition (CVPR), 2015. 6
- [52] Surat Teerapittayanon, Bradley McDanel, and Hsiang-Tsung Kung. BranchyNet: Fast Inference via Early Exiting from Deep Neural Networks. In 2016 23rd International Conference on Pattern Recognition (ICPR), pages 2464–2469. IEEE, 2016. 2, 3, 6, 7, 8, 12, 13
- [53] Andreas Veit and Serge Belongie. Convolutional Networks with Adaptive Inference Graphs. In European Conference on Computer Vision (ECCV), pages 3–18, 2018. 2
- [54] Tuan-Hung Vu, Himalaya Jain, Maxime Bucher, Matthieu Cord, and Patrick Pérez. ADVENT: Adversarial Entropy Minimization for Domain Adaptation in Semantic Segmentation. In IEEE Conference on Computer Vision and Pattern Recognition (CVPR), pages 2517–2526, 2019. 5
- [55] Xin Wang, Fisher Yu, Zi-Yi Dou, Trevor Darrell, and Joseph E Gonzalez. SkipNet: Learning Dynamic Routing in Convolutional Networks. In European Conference on Computer Vision (ECCV), pages 409–424, 2018. 2
- [56] Yulong Wang, Xiaolu Zhang, Xiaolin Hu, Bo Zhang, and Hang Su. Dynamic Network Pruning with Interpretable Layerwise Channel Selection. In AAAI Conference on Artificial Intelligence (AAAI), pages 6299–6306, 2020. 2
- [57] Huikai Wu, Junge Zhang, Kaiqi Huang, Kongming Liang, and Yu Yizhou. FastFCN: Rethinking Dilated Convolution in the Backbone for Semantic Segmentation. In arXiv preprint arXiv:1903.11816, 2019. 2
- [58] Yanzhao Wu, Ling Liu, Juhyun Bae, Ka-Ho Chow, Arun Iyengar, Calton Pu, Wenqi Wei, Lei Yu, and Qi Zhang. Demystifying Learning Rate Policies for High Accuracy Training of Deep Neural Networks. In IEEE International Conference on Big Data (Big Data), pages 1971–1980, 2019. 12
- [59] Zuxuan Wu, Tushar Nagarajan, Abhishek Kumar, Steven Rennie, Larry S Davis, Kristen Grauman, and Rogerio Feris. BlockDrop: Dynamic Inference Paths in Residual Networks. In IEEE Conference on Computer Vision and Pattern Recognition (CVPR), pages 8817–8826, 2018. 2
- [60] Ji Xin, Raphael Tang, Jaejun Lee, Yaoliang Yu, and Jimmy Lin. DeeBERT: Dynamic Early Exiting for Accelerating BERT Inference. In 58th Annual Meeting of the Association for Computational Linguistics (ACL), pages 2246–2251, 2020. 2
- [61] Qunliang Xing, Mai Xu, Tianyi Li, and Zhenyu Guan. Early Exit Or Not: Resource-Efficient Blind Quality Enhancement for Compressed Images. In European Conference on Computer Vision (ECCV), 2020. 2
- [62] Huazhe Xu, Yang Gao, Fisher Yu, and Trevor Darrell. End-to-end learning of driving models from large-scale video datasets. In IEEE Conference on Computer Vision and Pattern Recognition (CVPR), pages 2174–2182, 2017. 1
- [63] Zhuliang Yao, Shijie Cao, Wencong Xiao, Chen Zhang, and Lanshun Nie. Balanced Sparsity for Efficient DNN Inference on GPU. In AAAI Conference on Artificial Intelligence (AAAI), volume 33, pages 5676–5683, 2019. 2
- [64] Juheon Yi and Youngki Lee. Heimdall: Mobile GPU Coordination Platform for Augmented Reality Applications. In Annual International Conference on Mobile Computing and Networking (MobiCom), 2020. 1
- [65] Changqian Yu, Jingbo Wang, Chao Peng, Changxin Gao, Gang Yu, and Nong Sang. BiSeNet: Bilateral Segmentation Network for Real-Time Semantic Segmentation. In European Conference on Computer Vision (ECCV), pages 325–341, 2018. 2, 13
- [66] Fisher Yu and Vladlen Koltun. Multi-Scale Context Aggregation by Dilated Convolutions. In International Conference on Learning Representations (ICLR), 2016. 2
- [67] Fisher Yu, Vladlen Koltun, and Thomas Funkhouser. Dilated Residual Networks. In IEEE Conference on Computer Vision and Pattern Recognition (CVPR), pages 472–480, 2017. 1, 2, 3, 6, 8, 12, 13
- [68] Zhihang Yuan, Bingzhe Wu, Zheng Liang, Shiwan Zhao, Weichen Bi, and Guangyu Sun. S2DNAS: Transforming Static CNN Model for Dynamic Inference via Neural Architecture Search. In European Conference on Computer Vision (ECCV), 2020. 2
- [69] E. Zakharov, Aleksei Ivakhnenko, Aliaksandra Shysheya, and V. Lempitsky. Fast Bi-layer Neural Synthesis of One-Shot Realistic Head Avatars. In European Conference on Computer Vision (ECCV), 2020. 1
- [70] Dewen Zeng, Weiwen Jiang, Tianchen Wang, Xiaowei Xu, Haiyun Yuan, Meiping Huang, Jian Zhuang, Jingtong Hu, and Yiyu Shi. Towards Cardiac Intervention Assistance: Hardware-aware Neural Architecture Exploration for Real-Time 3D Cardiac Cine MRI Segmentation. In ACM/IEEE International Conference on Computer-Aided Design (ICCAD), 2020. 2
- [71] Linfeng Zhang, Jiebo Song, Anni Gao, Jingwei Chen, Chenglong Bao, and Kaisheng Ma. Be your Own Teacher: Improve the Performance of Convolutional Neural Networks via Self Distillation. In IEEE International Conference on Computer Vision (ICCV), pages 3713–3722, 2019. 2, 4, 6, 7, 12
- [72] Linfeng Zhang, Zhanhong Tan, Jiebo Song, Jingwei Chen, Chenglong Bao, and Kaisheng Ma. SCAN: A Scalable Neural Networks Framework Towards Compact and Efficient Models. In Advances in Neural Information Processing Systems (NeurIPS), 2019. 2, 4, 6, 7, 12
- [73] Hengshuang Zhao, Xiaojuan Qi, Xiaoyong Shen, Jianping Shi, and Jiaya Jia. ICNet for Real-Time Semantic Segmentation on High-Resolution Images. In European Conference on Computer Vision (ECCV), pages 405–420, 2018. 1, 2, 13
- [74] Hengshuang Zhao, Jianping Shi, Xiaojuan Qi, Xiaogang Wang, and Jiaya Jia. Pyramid Scene Parsing Network. In IEEE Conference on Computer Vision and Pattern Recognition (CVPR), pages 2881–2890, 2017. 2
- [75] Zhi Zhou, Xu Chen, En Li, Liekang Zeng, Ke Luo, and Junshan Zhang. Edge Intelligence: Paving the Last Mile of Artificial Intelligence with Edge Computing. Proceedings of the IEEE, 107(8):1738–1762, 2019. 1

Supplementary Material

In the supplementary material of our paper, we provide some extra details on the experimental setup of our evaluation, as well as additional qualitative and quantitative data that further showcase the quality of results from Multi-Exit Semantic Segmentation (MESS) networks and how different training/inference schemes translate in practice.

5.1. Experimental Configuration

5.1.1 Training Protocol and Hyperparameters

All MESS and baseline models are optimised using SGD, starting from ImageNet [9] pre-trained backbones. The initial learning rate is set to $lr_0=0.02$ and poly lr-schedule ($lr_0 \cdot (1 - \frac{iter}{total\ iter})^{pow}$) [58] with $pow=0.9$ is employed. Training runs over 60K iterations in all datasets. Momentum is set to 0.9 and weight decay to 10^{-4} . We re-scale all images to a dataset-dependent base resolution b_R . During training we conduct the following data augmentation techniques: random re-scaling by $0.5\times$ to $2.0\times$, random cropping (size: $0.9\times$) and random horizontal flipping ($p = 0.5$). For Knowledge Distillation, we experimentally set α to 0.5.

5.1.2 Datasets

MS COCO: MS COCO forms one of the largest datasets for dense seen understanding tasks. Thereby, it acts as common ground for pre-training semantic segmentation models, across domains. Following common practice for semantic segmentation, we consider only the 20 semantic classes of PASCAL VOC [10] (plus a background class), and discard any training images that consist solely of background pixels. This results in 92.5K training and 5K validation images. We set b_R for COCO to 520×520 .

PASCAL VOC: PASCAL VOC (2012) comprises the most broadly used benchmark for semantic segmentation. It includes 20 foreground object classes (plus a background class). The original dataset consists of 1464 training and 1449 validation images. Following common practise we adopt the augmented training set provided by [16], resulting in 10.5K training images. For PASCAL VOC, b_R is set (equally to MS COCO) to 520×520 .

5.1.3 Baselines

To compare our work’s performance with the state-of-the-art, we evaluate against the following baselines:

- **E2E SOTA:** The SOTA end-to-end training method for early-exit classification networks, introduced by MSD-Net [20] and BranchyNet [52]. We have adapted this method for segmentation.
- **Frozen SOTA:** The SOTA frozen-backbone training method for early-exit classification networks, proposed

by SDN [24] and HAPI [26]. We have adapted this method for segmentation.

- **SelfDistill:** The SOTA self-distillation approach for early-exit classification networks, utilised in [72, 47, 71]. We have adapted this method for segmentation.
- **DRN:** Dilated Residual Networks [67], the leading approach for re-using classification pre-trained CNNs as backbones for semantic segmentation. We use an FCN head at the end.
- **DLBV3:** DeepLabV3 [67, 7], one of the SOTA semantic segmentation networks. We target the DRN-50 backbone variant.
- **segMBNetV2:** The lightweight MobileNetV2 segmentor presented in [49] with a FCN head.
- **LC:** The SOTA early-exit segmentation work Deep Layer Cascade [29]. LC proposes a pixel-wise adaptive propagation in early-exit segmentation networks, with confident pixel-level predictions exiting early.

5.1.4 Implementation Details

Training Process: MESS instances are built on top of existing segmentation networks, spanning all across the workload spectrum in the literature, i.e. from the computationally heavy [6] to the lightweight [49]. Through MESS, SOTA networks can be further optimised for deployment efficiency, demonstrating complementary performance gains by saving computation on easier samples. A key characteristic of the proposed two-stage MESS training scheme, is that it effectively preserves the accuracy of the final (baseline) exit, while boosting the attainable results to earlier segmentation exits. This is achieved by bringing together elements from both the end-to-end and frozen-backbone training approaches (Sec. 3.3.1). Thus, we consider the employed training scheme disentangled from the attainable comparative results, as long as both the baseline and the corresponding MESS instances share the same training procedure. As such, in order to preserve simplicity in this work, we use a straightforward training scheme, shared across all networks and datasets, and refrain from exotic data augmentation, bootstrapping and multi-stage pre-training schemes that can be found in accuracy-centric approaches.

Inference Process: The main optimisation objective of this work is deployment efficiency. This renders impractical many popular inference strategies that are broadly utilised in approaches from the literature that optimise solely for accuracy, as they introduce prohibitive workload overheads. As such, in this work, we refrain from the use of ensembles, multi-grid and multi-scale inference, image flipping, etc. Instead, in the context of this work, both MESS and baseline networks employ a straightforward single-pass inference scheme, across all inputs.

5.2. MESS Configuration

In order to convert a given segmentation network to MESS, we first profile the workload/latency of the provided backbone, to identify N candidate exit points (Sec. 3.1). Fig. 6 illustrates the outcome of this analysis for a DRN-50 model.

Our proposed framework co-optimises the number, placement and architectural configuration of exits of the resulting MESS instances, as well as the confidence thresholds, th_i^{pix} and th_i , for the case of input-dependent inference, through an automated search methodology. This search methodology is conditioned by the user to support different use-cases imposing varying requirements and/or constraints in the speed-accuracy profile of the resulting MESS network. Such requirements/constraints are incorporated to our framework as an optimisation objective (obj) in the following form:

$$obj : \{search\text{-}target \mid requirement, inference\text{-}setting\} \quad (9)$$

where $search\text{-}target \in \{min\text{-}cost(s) \text{ or } max\text{-}acc(s)\}$ and $requirement \in \{cost(s) \leq th_{cost} \text{ or } acc(s) \geq th_{acc}\}$ according to the search-target. The framework supports $\{budgeted, anytime \text{ and } input\text{-}dependent\}$ inference as inference-settings, each of which imposes a different formulation for the workload/latency cost during inference. Table 5 formally provides the cost function (used in Eq. (4) and (5)) for MESS configuration search under each of the supported inference settings.

5.3. MESS Efficiency Aspects

MESS networks and the associated proposed framework demonstrate pronounced efficiency on various aspects of their design, training and deployment journey.

Training Efficiency: Our MESS training scheme allows for the backbone networks to be trained once, in an exit-aware manner. Thereafter, different early-exit architectures can be attached and trained by keeping the weights of the backbone frozen. This approach enables for the early exits to be effectively trained with high accuracy without sacrificing the accuracy of the final exit, hence bringing together the benefits of both end-to-end and frozen-backbone training schemes. On top of this, our 2-stage training approach allows the decoupling of early-exit training from the rest of the network, in turn enabling the efficient training of various early-exit architectural setups through the 2nd stage of our training scheme alone. Tested on a 32 design-point search space, our approach reduces the training time by $3.1\times$ (in GPU hours) compared to the single-stage end-to-end approach.

Search Efficiency: The aforementioned property also applies to the inference stage, where early-exits with different architectural configurations can be seamlessly interchanged across the shared backbone network in a plug-and-play manner. This offers great flexibility for post-

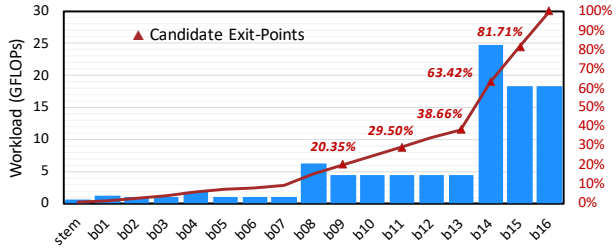


Figure 6: Workload breakdown analysis and exit-points identification on a DRN-50 [67] backbone.

training adaptation of MESS networks, targeting deployment to different devices or applications with varying accuracy/latency/memory requirements. Consequently, MESS networks are presented with the important advantage of remaining adaptable without the need to re-train. In contrast, networks that support dynamic inference through trainable gating mechanisms [30] or are compressed through NAS-based methods [34], exploit the user-provided deployment requirements during training as part of their custom loss functions, and therefore cannot be adapted for deployment to different devices/applications afterwards.

Inference Efficiency: MESS networks explore the dimension of input-dependent inference for semantic segmentation, aiming to obtain complementary performance gains by following a shorter computation path on easier samples. Therefore, the attainable results are model-agnostic and remain orthogonal to efficient segmentation network design through hand-crafted [73, 65, 49] or NAS-based [4, 34, 42] methodologies. Simultaneously, the MESS framework can convert existing segmentation CNNs to a MESS network in an automated manner, improving their efficiency through the input-dependent inference paradigm. As a result, MESS networks can follow the rapid progress in deep-learning-based segmentation architectures, by constantly applying the MESS framework over new and more accurate models.

Furthermore, compared to a naive adoption of classification-based approaches that employ a uniform exit architecture across the depth of the backbone [20, 52, 24, 26], MESS networks provide a significantly improved performance-accuracy trade-off that pushes the limits of efficient execution for semantic segmentation, by providing a highly customisable architectural configuration space, searched through the automated framework. Fig. 7 illustrates the per-label accuracy of multi-exit network instances. More specifically, on the left side we depict baseline networks using a uniform exit architecture of FCN heads at each candidate exit point. In contrast, on the right side we examine MESS networks incorporating a customised exit placement and architecture, configured in view of requirements ranging between $1\times$ and $4.5\times$ lower latency compared to the original network.

Table 5: Cost functions used for assessing the workload or latency of candidate MESS points during search, for budgeted, anytime and input-dependent deployment settings. b_i is the i -th block in the MESS network’s backbone; K_n is the block ordinal of the n -th head; $\mathcal{S}_{\text{exit}}^{*n} \in \mathcal{S}_{\text{exit}}^n$ is the selected architecture for the n -th exit; p_n is the percentage of samples in the calibration set propagated to the n -th exit.

Inference	$cost(s)$
Final-Only	$cost(b_{1:K_N}) + cost(\mathcal{S}_{\text{exit}}^{*N})$
Budgeted	$cost(b_{1:K_n}) + cost(\mathcal{S}_{\text{exit}}^{*n}), n \leq N$
Anytime	$cost(b_{1:K_N}) + \sum_{n=1}^N cost(\mathcal{S}_{\text{exit}}^{*n})$
Input-Dep.	$\sum_{n=1}^N p_{n-1} \cdot (cost(b_{K_{n-1}:K_n}) + cost(\mathcal{S}_{\text{exit}}^{*n})), K_0=0, p_0=1$

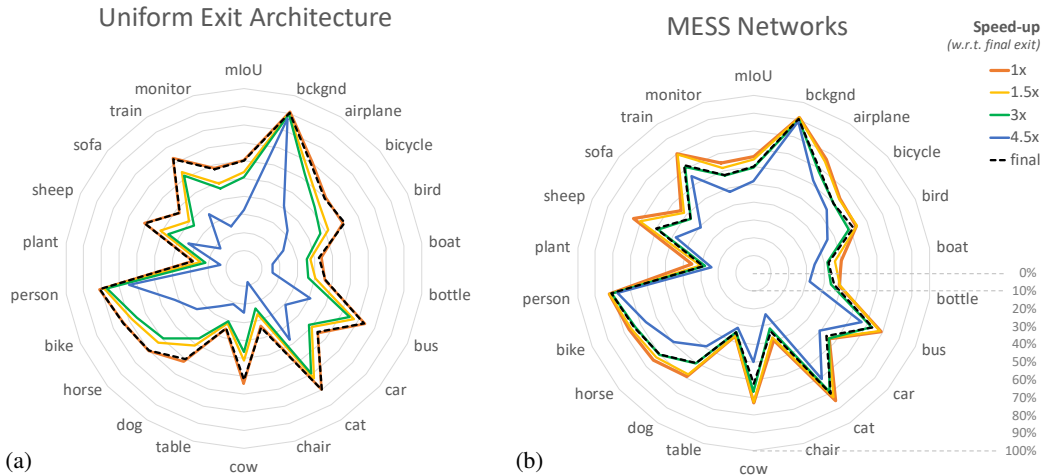


Figure 7: Per label IoU accuracy on MS COCO Validation Set of (a) uniform architecture early-exit networks and (b) specifically tuned MESS networks, for different latency goals (expressed as speed-ups with respect to the final exit), for ResNet50. Each of the concentric spider graphs defines a distribution of exit rates over different heads, based on the confidence threshold determined by our search. The graphs have value both when studied in isolation, so as to monitor the behaviour of early exits across labels, and in comparison, to understand what our principled design approach offers.

5.4. Qualitative Evaluation

Fig. 8, we demonstrates the quality-of-result for progressive segmentation outputs through a MESS network, for certain samples from MS COCO and PASCAL VOC. Table 6 shows the respective accuracies for the same set of images, along with the selected output, based on our exit policy.

Subsequently, Fig. 9 tells the story from a different standpoint, where we showcase how confident an exit of a MESS network is about its predictions. Concretely, we illustrate the (per-pixel) confidence heatmap for an early segmentation head and the final exit for certain samples of

the same datasets, with and without Eq. (8). This demonstrates how our confidence-based mechanism works in the realm of semantic segmentation and the contribution our edge smoothing technique in the confidence of predictions along object edges. Similarly, Table 7 shows the single (per-image) confidence values for each prediction, obtained both through a baseline and the proposed method.

Last, Fig. 10 depicts the qualitative difference of semantic map outputs with and without the proposed distillation mechanism incorporated during training. The two samples of the figure show clearly the kind of per-pixel prediction errors that our PFD scheme tries alleviate.

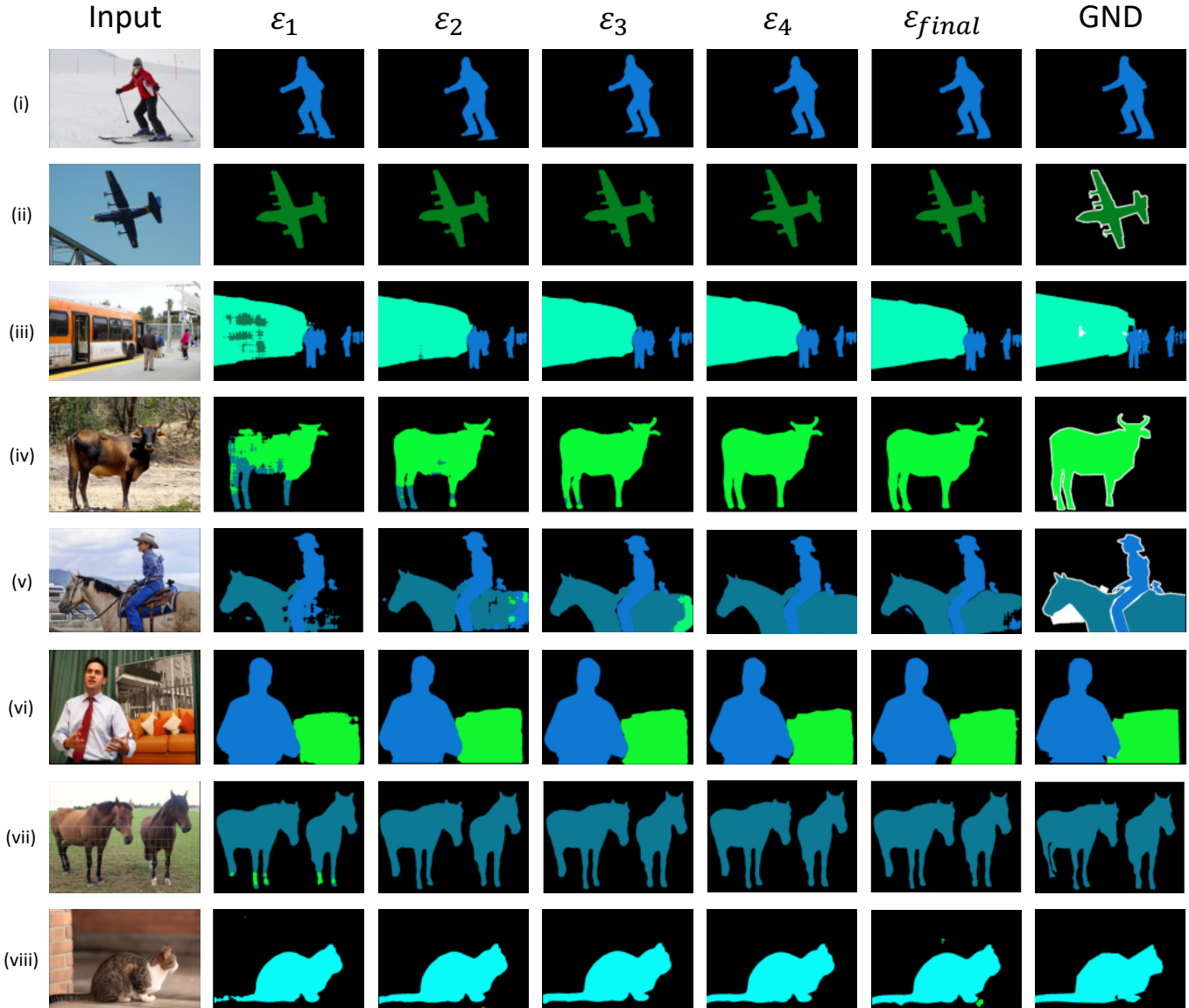


Figure 8: Visualisation of semantic segmentation per-exit outputs of MESS ResNet50 for specific samples from MS COCO and PASCAL-VOC. The first column represents the input image and last the ground truth labels. Intermediate columns represent the output per exit head.

Table 6: Semantic segmentation per-exit accuracy for samples of Fig. 8 from MS COCO and PASCAL-VOC Validation Set. mIoU represents the normalised mean IoU per image and pAcc the pixel-accuracy (excl. True Positives on background class) for each exit head. We denote the selected exit for each sample, determined by the proposed MESS exit policy, with **bold** font. Different exits have different confidence thresholds, selected during search, so as to lead to ≤ 1 pp of accuracy degradation.

Sample	ϵ_1		ϵ_2		ϵ_3		ϵ_4		ϵ_{final}	
	mIoU	pAcc	mIoU	pAcc	mIoU	pAcc	mIoU	pAcc	mIoU	pAcc
(i)	94.79%	90.70%	95.91%	92.69%	95.90%	92.67%	95.83%	92.53%	95.82%	92.53%
(ii)	92.89%	86.78%	90.40%	82.12%	91.93%	84.98%	93.32%	87.58%	93.35%	87.62%
(iii)	84.61%	82.30%	88.68%	92.29%	88.98%	92.77%	89.16%	93.07%	88.19%	93.07%
(iv)	83.18%	68.73%	95.67%	91.82%	98.51%	97.58%	99.03%	98.53%	98.97%	98.45%
(v)	73.06%	65.14%	81.11%	82.06%	96.68%	90.01%	97.64%	98.31%	90.78%	90.27%
(vi)	92.47%	92.87%	95.24%	95.34%	95.46%	95.54%	95.43%	95.53%	95.25%	95.34%
(vii)	93.07%	89.88%	94.49%	92.72%	94.59%	92.87%	94.56%	92.85%	94.54%	92.78%
(viii)	93.98%	90.75%	95.58%	93.09%	95.47%	93.12%	92.98%	93.89%	95.31%	92.10%

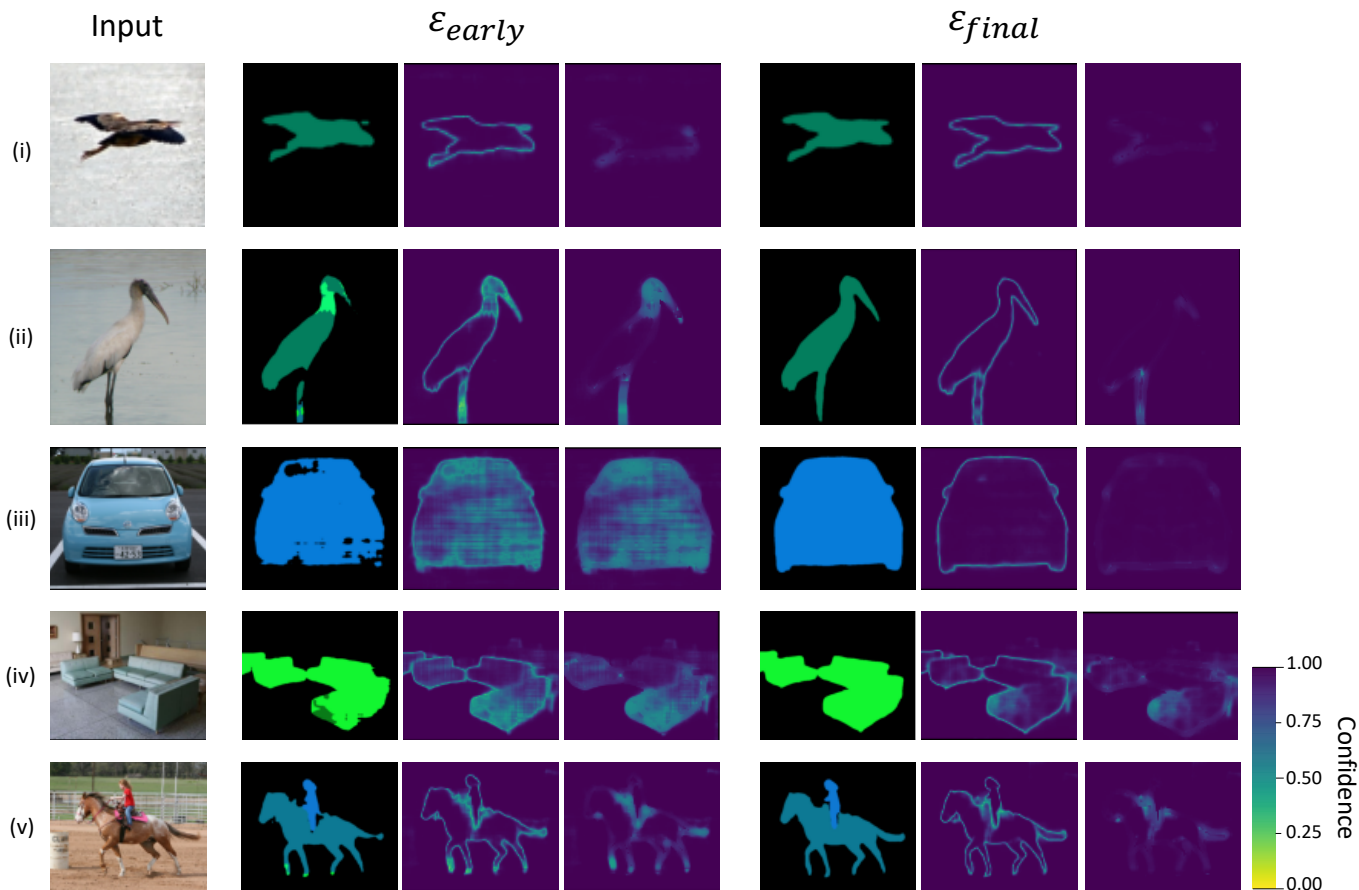


Figure 9: Per pixel confidence maps for an early and the final segmentation heads for ResNet50 with and without integrating Eq. (8). A solid purple colour is illustrating the best possible result, where the MESS network is most confident about the per pixel labels. With our edge smoothing technique (Section 3.4.2) we witness a more pragmatic confidence estimation for predictions along the edges of objects for both exits. This is especially important for early heads of MESS networks, as it helps distinguishing between “truly” under-confident and edge-rich predictions, leading to higher early-exit rates with respective latency gains.

Table 7: Per image confidence values for samples illustrated in Fig. 9, reduced from the respective per pixel confidence maps, through a baseline confidence averaging approach and the proposed technique (considering the percentage of confident pixels at the output) with and without integrating the semantic edge confidence smoothing of Eq. (8). Using the proposed per-image confidence estimation methodology for dense predictions, a better separation is achieved between confident predictions (corresponding to higher quality-of-result outputs) and less confident predictions (prone to semantic errors).

Sample	\mathcal{E}_{early}			\mathcal{E}_{final}		
	mean(c^{map})	Eq. (6)	Eq. (6) + (8)	mean(c^{map})	Eq. (6)	Eq. (6) + (8)
(i)	0.990	0.975	0.999	0.992	0.977	1.000
(ii)	0.968	0.920	0.946	0.983	0.951	0.988
(iii)	0.871	0.595	0.599	0.983	0.958	0.999
(iv)	0.905	0.725	0.734	0.958	0.874	0.918
(v)	0.967	0.913	0.939	0.975	0.924	0.966

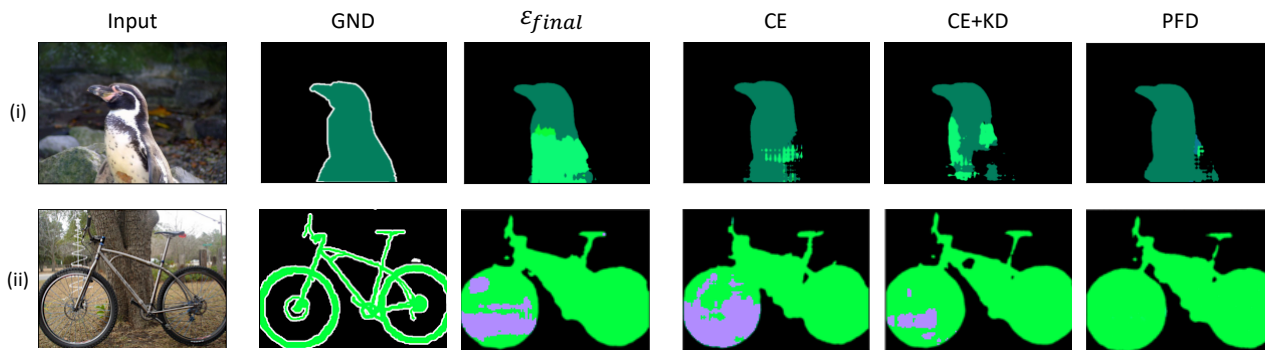


Figure 10: Qualitative examples of semantic segmentation with different distillation schemes on ResNet50. From left to right we see the input image, the ground truth semantic map, the output of the final exit (\mathcal{E}_{final}) and the output of an early exit without distillation (CE), with baseline distillation (CE+KD) and with the proposed positive filtering distillation (PFD) approach. The proposed scheme aims to control the flow of information to early exits in knowledge distillation, “paying more attention” to pixels that are correctly predicted by the final exit during training, while avoiding to use contradicting CE and KD reference signals in the remainder of the image. The provided samples illustrate the kind of information that can be learned by means of the PFD scheme, even in the case of the original final exit being incorrect for certain pixels.